

THE 1998 OUTBURST OF XTE J1550–564:  
A MODEL BASED ON MULTIWAVELENGTH OBSERVATIONS

K. WU<sup>1,2</sup>, R. SORIA<sup>1</sup>, D. CAMPBELL-WILSON<sup>2</sup>, D. HANNIKAINEN<sup>3</sup>, B. A. HARMON<sup>4</sup>,  
R. HUNSTEAD<sup>2</sup>, H. JOHNSTON<sup>2</sup>, M. MCCOLLOUGH<sup>4</sup>, AND V. MCINTYRE<sup>2,5</sup>

kw@mssl.ucl.ac.uk; rs1@mssl.ucl.ac.uk

to appear in *ApJ*, vol. 564, Jan 2002

ABSTRACT

The 1998 September outburst of the black-hole X-ray binary XTE J1550–564 was monitored at X-ray, optical and radio wavelengths. We divide the outburst sequence into five phases and discuss their multiwavelength properties. The outburst starts with a hard X-ray spike, while the soft X-ray flux rises with a longer timescale. We suggest that the onset of the outburst is determined by an increased mass transfer rate from the companion star, but the outburst morphology is determined by the distribution of specific angular momentum in the accreting matter. The companion in XTE J1550–564 is likely to be an active magnetic star, with a surface field strong enough to influence the dynamics of mass transfer. We suggest that its magnetic field can create a magnetic bag capable of confining gas inside the Roche lobe of the primary. The impulsive rise in the hard X-rays is explained by the inflow of material with low angular momentum onto the black hole, on a free-fall timescale, when the magnetic confinement breaks down. At the same time, high angular momentum matter, transferred via ordinary Roche-lobe overflow, is responsible for the formation of a disk.

*Subject headings:* accretion, accretion disks — black hole physics — stars: binaries: close — stars: magnetic field — stars: individual: XTE J1550–564 — X-rays: stars

1. INTRODUCTION

Many soft X-ray transients (SXTs) are binaries containing a low-mass star transferring material to a black hole. SXT outbursts are usually attributed to accretion-disk or mass-transfer instabilities, and show a variety of patterns and properties. It has been suggested that the companion star may also play an important role, depending on its evolutionary status and its response to irradiative heating. (See e.g. Tanaka & Lewin 1995 for a review.) The diversity of the outburst behavior in SXTs may therefore arise from the different nature of their companion stars.

XTE J1550–564 was discovered on MJD 51063 (1998 Sep 7; MJD=JD–2,400,000.5) by the All-Sky Monitor (ASM) on board *RXTE* (Smith 1998) and by the Burst and Transient Source Experiment (BATSE) on board *CGRO* (Wilson et al. 1998). The optical counterpart was identified shortly afterwards (Orosz, Bailyn & Jain 1998), and a radio source was found at the optical position (Campbell-Wilson et al. 1998). From the optical ellipsoidal modulations, an orbital period of  $1.541 \pm 0.009$  d was inferred (Jain et al. 2001). For a detailed analysis of the X-ray spectral behavior of the source during the 1998 outburst, based on RXTE observations, see Sobczak et al. (2000).

2. X-RAY AND RADIO OBSERVATIONS

The BATSE experiment onboard *CGRO* (Fishman et al. 1989) was used to monitor the hard X-ray emission from XTE J1550–564. The BATSE Large Area Detectors (LADs) can monitor the whole sky almost continuously in the energy range of 20 keV – 2 MeV with a typical

daily 3 sigma sensitivity of better than 100 mCrab. Detector counting rates with a timing resolution of 2.048 seconds are used for our data analysis. To produce the XTE J1550–564 light curve, single step occultation data were taken using a standard Earth occultation analysis technique used for monitoring hard X-ray sources (Harmon et al. 1992). Interference from known bright sources was removed. A spectral analysis of the BATSE data indicated that the data were well fitted by a power law with a spectral index of –3.0. The single occultation step data were then fitted with a power law with this index to determine daily flux measurements in the 20–100 keV band.

The initial detection of XTE J1550–564 as a radio source was made on MJD 51065 with the Molonglo Observatory Synthesis Telescope (MOST) at 843 MHz (Campbell-Wilson et al. 1998). The evolution of the radio source was monitored with MOST over the following 27 days, using partial synthesis observations with integration times ranging from 1 to 9 hours; calibration sources were PKS B1421–490 and B1934–638. Flux density measurements were complicated by sidelobes from the nearby radio-bright supernova remnant G326.3–1.8 (Whiteoak & Green 1996), necessitating an image differencing approach using a matched reference image of the field obtained earlier in 1998 when XTE J1550–564 was quiescent. The flux density estimates are given in Table 1, with the errors being the quadrature combination of a 3 mJy rms noise contribution and a 3% calibration uncertainty. Other radio data obtained at higher frequencies with the Australia Telescope Compact Array, together with VLBI im-

<sup>1</sup> MSSL, University College London, Holmbury St. Mary, Dorking, Surrey, RH5 6NT, UK

<sup>2</sup> School of Physics, University of Sydney, NSW 2006, Australia

<sup>3</sup> Department of Physics and Astronomy, University of Southampton, Southampton, SO17 1BJ, UK

<sup>4</sup> SD50, NASA-MSFC, Huntsville, AL 35812, USA

<sup>5</sup> ATNF, CSIRO, PO Box 76, Epping, NSW 1710, Australia

ages from the Australian Long Baseline Array, will be presented elsewhere (Hannikainen et al. 2002, in preparation); preliminary results are given in Hannikainen et al. (2001).

### 3. THE 1998 OUTBURST SEQUENCE

Figure 1 shows the UV/optical/IR, hard/soft X-ray and radio lightcurves of XTE J1550–564 between MJD 51050 and 51155. The data in the top panel of Fig. 1 are from Jain et al. (1999), and Sanchez-Fernandez et al. (1999). We divide the 1998 outburst into five phases, named after the corresponding stages in the *RXTE*/ASM X-ray light curve (bottom panel of Fig. 1): (1) fast rising, (2) slow rising, (3) flare, (4) post-flare plateau, and (5) X-ray decline.

*Phase 1: fast rise (MJD 51063–51064.5)* The onset of the outburst is characterised by an impulsive rise in the hard X-rays. The BATSE (20–100 keV) flux reached about  $0.3 \text{ ph cm}^{-2} \text{ s}^{-1}$  within one day, and peaked at about  $0.4 \text{ ph cm}^{-2} \text{ s}^{-1}$  the next day. From *RXTE*/PCA and *RXTE*/HEXTE data (Wilson & Done 2001), the 20–200 keV flux peaks at  $\approx 1.7 \times 10^{37} \text{ erg s}^{-1}$ , for a distance of 2.5 kpc (Sanchez-Fernandez et al. 1999). Assuming a “canonical” efficiency  $\eta \sim 0.1$ , the total accreted mass required to account for the initial hard X-ray burst is  $\lesssim 10^{23} \text{ g}$ . In fact, such high values of  $\eta$  are more appropriate for standard disk accretion. Hot advective flows in the inner region, where the hard X-rays are likely to be emitted, are radiatively inefficient, especially if the inflowing matter carries a large radial velocity. For  $\eta \sim 10^{-3}–10^{-4}$  (Quataert & Narayan 1999), the required mass would be  $10^{25}–10^{26} \text{ g}$ .

The soft X-rays showed an exponential-like rise: the *RXTE*/ASM (2–12 keV) count rate increased from 2 to  $40 \text{ ct s}^{-1}$ , with an e-folding timescale  $\lesssim 0.5 \text{ d}$ . The optical brightness reached ( $V, I$ )  $\approx (16.7, 14.6)$  (Jain et al. 1999), with the possibility that peak brightness had occurred before the optical counterpart was identified. The optical colours were redder than in the other phases, but the X-ray spectrum was harder (Wilson & Done 2001). Archival data from the MOST at 843 MHz showed no obvious detection of radio emission before the outburst.

*Phase 2: slow rise (MJD 51064.5–51074)* This phase can be divided into two stages, (A) MJD 51064.5–51068.5 and (B) 51068.5–51074, based on the rising timescales of the soft X-rays. The *RXTE*/ASM count rate increased from 40 to  $120 \text{ ct s}^{-1}$  with an e-folding timescale  $\approx 3 \text{ d}$  in stage A, slowing down markedly through stage B with an e-folding timescale  $\gtrsim 12 \text{ d}$ . In contrast, the hard X-ray flux dropped rapidly: it had fallen to around half of the Phase 1 peak value by the end of stage A (MJD 51068.5), and remained essentially constant throughout stage B. Table 2 lists the hard and soft X-ray luminosity over Phases 1 and 2, inferred from the *RXTE*/PCA data (Wilson & Done 2001).

Radio emission became detectable, with MOST flux densities at a level of 10–30 mJy. Optical emission remained steady, with ( $U, B, V, I$ )  $\approx (18, 18, 17, 15)$  (Sanchez-Fernandez et al. 1999; Jain et al. 1999).

*Phase 3: flare (MJD 51074–51080)* There was a strong flare in all wavebands. Within one day the *RXTE*/ASM count rate rose rapidly from 200 to  $500 \text{ ct s}^{-1}$ . After peaking on MJD 51076, it dropped back to the  $200\text{-ct s}^{-1}$  level

in one day, and then to  $100 \text{ ct s}^{-1}$  in another two days. The BATSE flux increased almost simultaneously with the soft X-rays, reaching a value of  $\sim 0.5 \text{ ph cm}^{-2} \text{ s}^{-1}$  within a day. It then dropped back to the  $0.2\text{-ph cm}^{-2} \text{ s}^{-1}$  level in the next day. Both the *RXTE*/ASM and BATSE lightcurves appear to be symmetric with respect to the flare peak in this phase, but differences in the rising and falling times are revealed in higher time-resolution BATSE data.

The radio flare peaked at MJD  $51077.8 \pm 0.1$ ,  $\sim 1.8 \text{ d}$  after the X-ray peak, with the flux density reaching 380 mJy at 843 MHz. The decay was slower than in the X-ray bands, taking four days to decline to the 100-mJy level, which is still about 5 times the pre-flare flux density. The optical flare showed a delay of approximately one day with respect to the X-ray flare, peaking on MJD 51077.05; the brightening was less than 0.8 mag in each of the  $B, V$  and  $I$  bands. The optical emission reddened during the flare (Jain et al. 1999).

*Phase 4: post-flare plateau (MJD 51080–51107)* The *RXTE*/ASM count rate showed some scatter around a mean level of  $\sim 120 \text{ ct s}^{-1}$ , while the BATSE flux remained steady at the  $0.2\text{-ph cm}^{-2} \text{ s}^{-1}$  level. The 843 MHz flux density continued to decline monotonically, reaching  $\sim 14 \text{ mJy}$  at MJD 51092, at which point the monitoring was stopped. The  $B, V$  and  $I$  brightness of the source faded steadily by  $\approx 0.04 \text{ mag d}^{-1}$  (Jain et al. 1999).

*Phase 5: X-ray decline (MJD 51107–51150)* Both the *RXTE*/ASM and the BATSE fluxes declined, with e-folding timescales  $\approx 11$  and  $9 \text{ d}$  respectively. The optical brightness of the source continued to fade, with  $B$  falling below 19.5 mag on MJD 51113 (Jain et al. 1999).

### 4. MAGNETIC NATURE OF THE COMPANION STAR

The 1.54-day orbital period together with the faintness of the quiescent optical counterpart suggest that XTE J1550–564 is a low-mass system. The companion star should be close to filling its Roche lobe, so that the mass transfer can be rapid enough to fuel the outbursts and sustain the subsequent soft state. The mean density of the companion star is therefore  $\approx 0.077 \text{ g cm}^{-3}$ , similar to that of early B main-sequence stars or G/K subgiants. The quiescent brightness and the observed colour differences favor a late-type subgiant.

There are two consequences of having a late-type subgiant companion in the system. Firstly, if we adopt a 1.5-day orbital period, and assume that a  $10\text{-}M_{\odot}$  black hole is powering isotropic emission of X-rays at 0.1 of the Eddington luminosity, the fraction of X-ray luminosity ( $\sim 10^{36} \text{ erg s}^{-1}$ ) intercepted by the companion star will be much greater than the intrinsic luminosity of the G/K subgiant companion ( $\sim 10^{33}–10^{35} \text{ erg s}^{-1}$ ). Irradiation by soft X-rays will cause surface evaporation and blanketing of the energy diffusing from the stellar interior. Irradiation by hard X-rays will result in the deposition of energy deep in the stellar envelope (e.g. Vilhu, Ergma & Fedorova 1994). A cool subgiant companion is therefore susceptible to irradiative heating and consequent instabilities.

Secondly, while the tidally-deformed stellar envelope can be locked in synchronous rotation with the orbit, the degenerate stellar core may not attain perfect rotational synchronism. The differential rotation leads to dynamo action and magnetic activity, similar to the situation in the RS

CVn systems, which are magnetic close binaries containing a G/K subgiant. For instance, in the well-studied RS CVn system HR 1099, with a 2.8-day orbital period, there is strong evidence (Donati et al. 1992, Vogt et al. 1999) that the K1 IV component harbours a multi-kilogauss global dipolar field.

Given that fast rotating isolated G/K subgiants (Schrijver & Pols 1993) and G/K subgiants in RS CVn systems are highly magnetically active, G/K subgiants in X-ray binaries can also be magnetic. A surface field strength of 1 kG, corresponding to a magnetic stress of  $4 \times 10^4 \text{ erg cm}^{-3}$ , is strong enough to influence the mass- and energy-transport process in the stellar atmosphere. By postulating a magnetic G/K subgiant companion for XTE J1550–564 we are implying a new scenario in which the outburst properties are determined not only by accretion-disk instabilities, mass-transfer instabilities and irradiative heating, but also by stellar magnetism.

## 5. THE PHENOMENOLOGY OF THE OUTBURST

Three remarkable features of the 1998 outburst of XTE J1550–564 are: (1) an impulsive rise in the hard X-rays, while the soft X-ray flux remained low at the onset of the outburst; (2) a subsequent giant flare that occurred almost simultaneously in both hard and soft X-rays about twelve days after the initial rise of the hard X-rays; (3) an exponential decay in the soft X-ray brightness at the end of Phase 5, with the same timescale as those seen in the 1999 and 2000 outbursts.

### 5.1. Impulsive inflow and hard X-ray burst

It is generally accepted that hard X-ray emission is not thermal emission from an accretion disk (whose maximum temperature is  $\sim 1 \text{ keV}$ ), but is produced by inverse Compton scattering of softer photons off highly energetic ( $E \sim 100 \text{ keV}$ ) electrons near the BH. Theoretical studies have shown that accretion of matter with low angular momentum tends to produce hard X-rays (Igmenshchev, Illarionov & Abramowicz 1999; Beloborodov & Illarionov 2000; Chakrabarti & Titarchuk 1995). The physical justification is that free-falling electrons in a quasi-spherical inflow can acquire kinetic energies  $\gtrsim 100 \text{ keV}$  as they approach the BH horizon. The kinetic energy of the infalling electrons powers the Comptonisation process, either directly (bulk-motion Comptonisation) or after it has been converted into thermal energy (thermal Comptonisation).

Impulsive hard X-ray bursts can occur if the injection of material is also impulsive and with a narrow distribution of angular momenta. We therefore argue that an impulsive injection of matter with low angular momentum was responsible for the initial hard X-ray spike in the 1998 outburst, and that this initial condition could have been a consequence of a magnetic companion star.

### 5.2. Magnetic bags around G/K stars

Extended regions of cool, optically-thin, magnetically confined material around a K star are a common feature of RS CVn systems. The typical scale-height of these prominences above the photosphere is about twice the stellar radius, implying a volume of  $\sim 10^{34}\text{--}10^{35} \text{ cm}^3$  for the confining region. Prominences evolve over timescales of days,

and contain at any given time a mass of  $\sim 10^{20} \text{ g}$  (Hall & Ramsey 1994).

We argue that the mass of cold, magnetically-confined gas can in fact be even higher in XTE J1550–564, when the magnetic companion star is close to filling its Roche lobe. The inner Lagrangian ( $L_1$ ) point is a saddle point where the gravitational force is negligible, and matter can be more easily lifted up from the photosphere of the companion star. Moreover, the gas is prevented from moving in any direction other than along the axis between the stars; at the same time, the magnetic field of the companion star restricts the flow along that axis. The gas mass builds up (over a timescale of a few days) until eventually the gas pressure overcomes the magnetic barrier (see Figure 2 for a cartoon picture of our model).

For magnetic confinement near  $L_1$ , the magnetic tension/stress must be greater than the gas pressure, implying a critical density for the confined matter:

$$\rho_c \approx \frac{\mu m_H B^2}{8\pi kT} \sim 2 \times 10^{-8} \text{ g cm}^{-3} \left( \frac{B}{1 \text{ kG}} \right)^2 \left( \frac{T}{10^4 \text{ K}} \right)^{-1}. \quad (1)$$

For the sizes of the confining regions in RS CVn systems, and if we assume uniform density, this corresponds to a mass upper limit of  $\sim 10^{26} \text{ g}$ . (If the gas accumulates near the loops' apices, the total mass may be less than this value when the confinement breaks down.) This is consistent with the accreted mass that is required to explain the initial hard X-ray burst (§3). By analogy with RS CVn systems, the confined gas in XTE J1550–564 may be located well beyond the  $L_1$  point, deep into the Roche lobe of the primary, but corotating with the binary. The mass loss rate of the secondary would then determine the time necessary to fill the magnetic bags.

At the start of an outburst, as the magnetic companion star is close to filling its Roche lobe, part of the photospheric layers is lifted and confined in a magnetic bag beyond the  $L_1$  point (low angular momentum component of the accretion flow), while another component starts to be transferred through the Lagrangian point (high angular momentum component). It is the low-angular momentum component that we believe is responsible for the peculiar hard X-ray spike seen in Phase 1, while the high-angular momentum component leads to the formation of the disk.

### 5.3. Quasi free-fall accretion

As the magnetic prominence evolves, the material confined beyond the  $L_1$  point tends to collect in the loop apex, until its density increases and it eventually bursts the magnetic dam, breaking free of the field. In a frame corotating with the orbit, the average initial angular momentum of the accreting matter with respect to the black hole is low, i.e., it is effectively in radial free-fall. In contrast, the angular momentum of the matter accreted via conventional Roche-lobe overflow is large, because the matter passing through the  $L_1$  point is transonic, and the accretion stream has a non-zero pitch angle (see Lubow & Shu 1975).

The low angular momentum component of the flow will deviate from near-radial only when approaching the black hole. When the infalling material encounters its centrifugal barrier in the vicinity of the hole, an accretion shock may be formed, converting the kinetic energy to radiation. The photons would then be upscattered by the hot

electrons, causing an outburst of hard X-rays. In an alternative scenario, the photons may be upscattered as they interact with the bulk motion of the infalling electrons. When the low-angular-momentum accreting material is depleted, the quasi-spherical inflow subsides, and the hard X-ray luminosity declines. At the same time, an accretion disk is formed at large radii by the matter transferred via Roche-lobe overflow. The steady building and expansion of the disk inwards via diffusion processes results in a gradual increase of the optical brightness and then of the soft X-ray luminosity, evident in Phases 1 and 2.

The *hard* X-rays can penetrate deep into the star, and deposit energy into the convective envelope, thus disturbing the thermal equilibrium of the star. The star must readjust its structure in response to the sudden heating, and it will expand until a new equilibrium is established. At the same time, *soft* X-ray irradiation causes an instantaneous heating of the upper stellar atmosphere, and hence a rapid increase in the atmospheric scale height. The timescale for thermal readjustment of the stellar envelope (up to a few weeks) is longer than the dynamic and thermal timescales of atmospheric activity induced by soft X-ray irradiation (Vilhu et al. 1994). Although both hard and soft X-ray irradiation will eventually cause an increase in the rate of mass transfer, there will be a delayed response from the companion star to the initial strong hard X-ray heating. The subsequent onset of a soft state is probably due to the subgiant regaining contact with its critical Roche surface, as a result of the delayed expansion caused by the hard X-ray heating.

#### 5.4. Trigger of the giant flare

During Phases 1 and 2 we have accretion of free-falling matter with low angular momentum at small radii, and accretion of matter with high angular momentum, via Roche-lobe overflow, at large radii. The former creates a hot, pressure-supported, sub-Keplerian “disk” or quasi-spherical region at small radii, growing outwards; the latter creates a Keplerian ring slowly diffusing inwards and outwards, forming a standard Shakura-Sunyaev disk. A discontinuity arises when the two accretion flows meet, and the inner boundary of the Keplerian disk is subject to a strong shear. We suggest that this leads to a sudden increase in mass transfer as the outer, denser, colder gas suddenly loses part of its angular momentum at this shear discontinuity, thereby triggering the giant soft and hard X-ray flare around MJD 51076 (Phase 3).

The initial hard X-ray burst in Phase 1 and the giant flare in Phase 3 have different soft X-ray properties. Moreover, the latter was accompanied by strong radio activity. Because of insufficient shear, the quasi-spherical accretion flow in Phase 1 is unlikely to amplify the seed magnetic field carried by the infalling matter significantly. Only after an accretion disk is formed will dynamo action become efficient and amplify the field. One possibility is that when the magnetic disk joins the sub-Keplerian inner region, and mass accretion suddenly increases (giant flare), the magnetic field is dragged rapidly towards the black-hole event horizon by the accreting matter. The field would be compressed and might reconnect, causing the expulsion of disk material and hence the formation of a radio flare/jet.

The small increase in optical brightness during the giant

X-ray flare is surprising. However, the heating of the companion star and of the accretion disk could have saturated due to strong X-ray irradiation during the previous phases, and the accretion disk may already have been extended to its outer tidal limit.

#### 5.5. Drainage of the accretion disk

Around MJD 51110, both the hard and soft X-ray luminosity began to decline exponentially, with the soft X-rays lagging the hard. The e-folding decay timescale is  $11.0 \pm 0.1$  d for *RXTE*/ASM and slightly shorter for BATSE. The corresponding decay timescales for the later outbursts in 1998/1999 and 2000 are almost identical:  $11.3 \pm 0.1$  and  $11.1 \pm 0.2$  d respectively (Figure 3).

The decline in the X-ray luminosity is therefore evidence of the drainage of the accretion disk. The timescale on which a disk is emptied is

$$t \approx \frac{R_d^2}{\nu} \sim \frac{1}{\nu} \left( \frac{0.6}{1+q} \right)^2 \left[ \left( \frac{P}{2\pi} \right)^2 GM_1(1+q) \right]^{2/3} \quad (2)$$

(Pringle 1981), where  $G$  is the gravitational constant,  $P$  the orbital period,  $M_1$  the black-hole mass,  $q$  ( $\equiv M_2/M_1$ ) the mass ratio,  $R_d$  the disk radius, and  $\nu$  the effective viscosity. A decay timescale of 11 days implies  $\nu \sim 2.3 \times 10^{17}$  cm<sup>2</sup> s<sup>-1</sup> if  $q \approx 0.1$ ,  $M_1 = 10 M_\odot$ . The effective viscosity is often expressed in terms of a constant parameter  $\alpha$  (Shakura & Sunyaev 1973):

$$\nu \approx \alpha H c_s \approx \alpha c_s^2 / \Omega, \quad (3)$$

where the sound speed  $c_s \approx (kT/m_p)^{1/2}$ , and the Keplerian angular velocity  $\Omega \approx 1.2 \times 10^{-3} (M/10 M_\odot)^{1/2} (R/10^{11} \text{ cm})^{-3/2}$  s<sup>-1</sup>. For temperatures  $10^4 \lesssim T \lesssim 10^5$  K, typical of the outer regions of the disk ( $R \approx R_d$ ), the observed timescale corresponds to an effective  $\alpha \sim 10$  at large radii.

## 6. A MODEL FOR THE ONSET OF THE OUTBURSTS

### 6.1. A subclass of BHC outbursts

A remarkable characteristic of the outburst behaviour of XTE J1550–564 is the presence of a sharp hard X-ray spike during the initial rise. This spectral behaviour is different to that observed in systems such as GRO J1655–40, GS 1354–64 or GX 339–4. The 1996 outburst of GRO J1655–40 started with a very soft state (Hynes et al. 1997), and the hard X-rays turned on about a month after the start of the outburst. In GS 1354–64, the soft and hard X-ray fluxes are well correlated during their rise and decline (Brocksopp et al. 2001). In GX 339–4, the soft and hard fluxes tend to be anticorrelated (Corbel et al. 2000). No initial hard X-ray spike is detected in any of those three systems.

In fact, XTE J1550–564 is not the only system showing a hard X-ray spike at the onset of an outburst. XTE J1859+226 (Wood et al. 1999; McCollough & Wilson 1999; Brocksopp et al. 2002) and XTE J2012+381 (Vasiliev et al. 2000) are two other good examples. In these three systems, the hard X-ray flux reached a maximum within the first day after detection, and then declined after about 4 days. The soft X-ray flux increased more steadily and at a slower pace, for  $\sim 10$  days. The similarity in the X-ray spectral properties of XTE J1550–564,

XTE J1859+226 and XTE J2012+381 can be seen from their hardness-ratios plots (Figure 4; data from the public *RXTE*/ASM archive). These systems probably belong to a subclass of BH transients, sharing a similar physical mechanism that gives rise to a strong hard X-ray spike at the onset of an outburst. A more detailed analysis of the hard X-ray properties of this type of systems will be presented elsewhere (Soria et al 2001, in preparation).

### 6.2. Formation of the hard X-ray spike

We propose that the difference between the outburst behaviour of systems like XTE J1550–564 and of the other BH transients is due to the difference in the relative angular momentum content of their accreting matter. Matter accreted via a stellar wind has a lower specific angular momentum than matter accreted via Roche-lobe overflow, and it has been suggested that the wind-fed systems and systems with Roche-lobe overflow have different preferential spectral states (Beloborodov & Illarionov 2001; Wu et al. 2001). There is also evidence that the accretion flow in BH X-ray binaries consists of separate components, each with a different distribution of angular momentum. Observations of 1E 1740–294, GRS 1758–258 and GX 339–4 (Smith, Heindl & Swank 2001) indicate that the delay of the soft component relative to the hard component (approximately equal to the difference between the viscous and the free-fall timescale) is more evident for systems with Roche-lobe overflow, i.e. those where a large accretion disk is present, and the high angular momentum component dominates. Shorter viscous delays were observed for wind-fed systems (e.g., Cyg X-1 in the hard state; Smith et al. 2001) where the low-angular momentum component dominates.

We attribute the presence of the hard X-ray spike in XTE J1550–564 to an inflow of accreting matter with low angular momentum, lasting over the first few days. The 3–200 keV X-ray spectrum of XTE J1550–564 at the peak of the initial hard phase (Wilson & Done 2001) is in fact very similar to the spectrum of Cyg X-1 in its hard state, consistent with the interpretation that the initial accretion flow in XTE J1550–564 was dominated by the low angular-momentum component.

### 6.3. Outburst morphology: role of the specific angular momentum

The hard and soft states of BHC outbursts are usually explained by models invoking an optically thick, geometrically thin accretion disk which is initially truncated in the inner region. The optical/IR flux comes mostly from the outer disk region. The soft X-ray flux rises on a viscous timescale as the disk grows inwards at the beginning of the outburst, and is therefore delayed with respect to the optical flux. At small radii, the accretion flow is hot and quasi-spherical. The hard X-rays are due to inverse-Compton scattering of soft photons from the disk or the companion star by highly energetic electrons in the hot quasi-spherical flow near the BH. When the quasi-spherical flow subsides and is replaced by the thin accretion disk extending down towards the innermost stable circular orbit of the BH, the system is observed in a high/soft state.

In our model, the outburst behaviour is determined by the mass-transfer rate (which determines the energetics

of the burst) and the angular momentum distribution of the accreting matter (which determines the initial spectral properties and the X-ray rise time). The inner, quasi-spherical flow is fed by the accretion of material with low angular momentum, while the disk is formed by accretion of high angular momentum matter transferred via Roche-lobe overflow. The initial hard X-ray emission is caused by a sudden injection of accreting matter with low angular momentum. When the injection ends and the supply of low-angular momentum accreting matter is depleted, the hard X-ray flux declines. In the case of XTE J1550–564, we attribute the decline of the low angular momentum accretion flow to the emptying of the magnetic reservoir. After the magnetic bags are drained, accretion proceeds only via Roche-lobe overflow.

Our model is in contrast to scenarios based on advection-dominated accretion flows (ADAF models; see Narayan & Yi 1995; Esin et al. 1997), in which spectral softening is attributed to the collapse of the hot, quasi-spherical flow into an optically thick disk when the mass accretion rate increases. An application of the ADAF model to the 1998 outburst of XTE J1550–564 has been presented by Wilson & Done (2001). The conventional ADAF scenarios do not explain why in some systems (such as XTE J1550–564) the hot inner region produces a strong hard X-ray spike before collapsing, while in other systems (such as GRO J1655–40) no such initial spike is observed. Moreover, the observed duration of the initial hard emission seems to be much longer than the timescale for the collapse of the hot flow in the conventional ADAF model (Wilson & Done 2001).

## 7. SUMMARY

We describe the morphology of the 1998 outburst of XTE J1550–564, dividing it into five phases. The outburst starts with a hard X-ray flare (peaking after  $\sim 1$  d); the same behaviour is observed in at least two other BHCs. We propose that the companion star in XTE J1550–564 is magnetically active, and its magnetic field creates a magnetic bag capable of confining  $\sim 10^{26}$  g of gas inside the Roche lobe of the primary, corotating with the binary. The impulsive rise in the hard X-rays is explained by the inflow of material with low angular momentum onto the black hole, on a free-fall timescale, when the magnetic confinement breaks down. At the same time, matter with higher angular momentum, transferred via Roche-lobe overflow, begins to form a Keplerian disk, responsible for the soft X-rays and optical emission. We suggest that the onset of the outburst is determined by an increased mass transfer rate from the companion star, but the outburst morphology is determined by the distribution of specific angular momentum in the accreting matter. When the inner boundary of the outer, denser Keplerian disk comes into contact with the inner sub-Keplerian hot region, the disk matter is subject to a strong shear and loses angular momentum. This disturbs the stability of the accretion disk, causes a sudden increase in the mass accretion rate, and is responsible for the observed giant X-ray flare and radio ejections. An identical timescale of 11 days is found for the decay of the soft X-ray flux in the three outbursts observed in this system, implying an effective viscosity  $\nu \sim 2.3 \times 10^{17}$  cm<sup>2</sup> s<sup>-1</sup> for the accretion disk.

We thank Celia Sanchez-Fernandez and Raj Jain for allowing us to use their optical data, and Colin Wilson for providing helpful information on his X-ray spectral fitting. We also thank the anonymous referee for providing useful suggestions on how to improve our paper. KW acknowledges support from the ARC Australian Research Fellowship and the PPARC-MSSL Visting Fellowship, and thanks Phil Charles for funding his visits to the University of Southampton. RS acknowledges support from the

University of Sydney during his visit there. DCH acknowledges the support of a UK PPARC postdoctoral research grant to the University of Southampton, and financial support from the Academy of Finland, and thanks the Astrophysics Department, Sydney University for hospitality during her visits. MOST is operated by Sydney University and supported by grants from the Australian Research Council.

## REFERENCES

- Beloborodov, A. M., & Illarionov, A. F. 2001, *MNRAS*, 323, 167  
 Brocksopp, C., Jonker, P. G., Fender, R. P., Groot, P. J., van der Klis, M., & Tingay, S. J. 2001, *MNRAS*, 323, 517  
 Brocksopp, C., et al. 2002, *MNRAS*, submitted  
 Campbell-Wilson, D., McIntyre, V., Hunstead, R. W., & Green, A. 1998, *IAUC* 7010  
 Chakrabarti, S., & Titarchuk, L. G. 1995, *ApJ*, 455, 623  
 Corbel, S., Fender, R. P., Tzioumis, A. K., Nowak, M., McIntyre, V., Durouchoux, P., & Sood, R. 2000, *A&A*, 359, 251  
 Donati, J.-F., et al. 1992, *A&A*, 265, 682  
 Esin, A. A., McClintock, J. E., & Narayan, R. 1997, *ApJ*, 489, 865; Erratum: *ApJ*, 500, 523  
 Fishman, G. J., et al. 1989, in *Proc. Gamma-Ray Observatory Science Workshop*, ed. N. Johnson (Greenbelt: Goddard Space Flight Center), 2-39  
 Hall, J. C., & Ramsey, L. W. 1994, *AJ*, 107, 1149  
 Hannikainen, D. C., Wu, K., Campbell-Wilson, D., Hunstead, R. W., Lovell, J., McIntyre, V., Reynolds, J., Soria, R., & Tzioumis, T. 2001, in *Proceedings of the 4th INTEGRAL Workshop (Alicante 2000)*, to be published in *ESA-SP* (2001); astro-ph/0102070  
 Harmon, B. A., et al. 1992, in *Proc. Compton Observatory Science Workshop*, ed. C.R. Shrader, N. Gehrels, and B. Dennis (Washington: NASA), 69  
 Hynes, R. I., Haswell, C. A., Shrader, C. R., Chen, W., Horne, K., Harlaftis, E. T., O'Brien, K., Hellier, C., & Fender, R. P. 1998, *MNRAS*, 300, 64  
 Igumenshchev, I. V., Illarionov, A. F., & Abramowicz, M. A. 1999, *ApJ*, 517, L55  
 Jain, R. K., Bailyn, C. D., Orosz, J. A., Remillard, R. A., & McClintock, J. E. 1999, *ApJ*, 517, 131  
 Jain, R. K., Bailyn, C. D., Orosz, J. A., McClintock, J. E., Sobczak, G. J., & Remillard, R. A. 2001, *ApJ*, 546, 1086  
 Lubow, S. H., & Shu, F. H. 1975, *ApJ*, 198, 383  
 McCollough, M. L., & Wilson, C. A. 1999, *IAUC* 7282  
 Narayan, R., & Yi, I. 1995, *ApJ*, 444, 231  
 Orosz, J. A., Bailyn, C. D., & Jain, R. K. 1998, *IAUC* 7009  
 Pringle, J. E. 1981, *ARA&A*, 19, 137  
 Quataert, E., & Narayan, R. 1999, *ApJ*, 520, 298  
 Sanchez-Fernandez, C. et al. 1999, *A&A*, 348, L9  
 Schrijver, C. J., & Pols, O. R. 1993, *A&A*, 278, 51  
 Smith, D. A. 1998, *IAUC* 7008  
 Smith, D. M., Heindl, W. A., & Swank, J. H. 2001, astro-ph/0103304  
 Sobczak, G. J., McClintock, J. E., Remillard, R. A., Cui, W., Levine, A. M., Morgan, E. H., Orosz, J. A., & Bailyn, C. D. 2000, *ApJ*, 544, 993  
 Tanaka, Y., Lewin, W. H. G. 1995, in *Lewin, W. H. G., van Paradijs, J. & van den Heuvel, E. P. J., eds, X-ray Binaries*, Cambridge University Press, Cambridge, p.126  
 Vasiliev, L., Trudolyubov, S., & Revnivtsev, M. 2000, *A&A*, 362, L53  
 Vilhu, O., Ergma, E., & Fedorova, A. 1994, *A&A*, 291, 842  
 Vogt, S. S., Hatzes, A., Misch, A. A., & Meurster, M. 1999, *ApJS*, 121, 589  
 Whiteoak, J. B. Z., & Green, A. J. 1996, *A&AS* 118, 329  
 Wilson, C. D., & Done, C. 2001, *MNRAS*, 325, 167  
 Wilson, C. A., Harmon, B. A., Paciesas, W. S., & McCollough, M. L. 1998, *IAUC* 7010  
 Wood, A., Smith, D. A., Marshall, F. E., & Swank, J. E. 1999, *IAUC* 7274

TABLE 1  
 MOST FLUX DENSITIES FOR XTE J1550–564 DURING THE 1998 OUTBURST

Time at mid-observation (MJD)	Flux density at 843 MHz (mJy)
51065.175	$12 \pm 3$
51066.156	$16 \pm 3$
51071.203	$27 \pm 3$
51073.193	$18 \pm 3$
51076.390	$168 \pm 6$
51077.298	$327 \pm 10$
51078.259	$375 \pm 12$
51079.318	$221 \pm 7$
51080.302	$155 \pm 6$
51081.210	$120 \pm 5$
51087.360	$20 \pm 3$
51092.177	$14 \pm 3$

TABLE 2  
X-RAY LUMINOSITY OF XTE J1550–564 DURING PHASES 1-2

Obs. date (MJD)	$L_{3-20 \text{ keV}} (10^{37} \text{ erg s}^{-1})$	$L_{20-200 \text{ keV}} (10^{37} \text{ erg s}^{-1})$	$L_{\text{bol}} (10^{37} \text{ erg s}^{-1})$
51063	0.67	1.67	3.41
51064	0.84	1.57	3.15
51065	1.49	1.59	4.41
51067	2.24	1.17	5.38
51072	2.96	0.83	8.13

Note. — *RXTE*/PCA plus *RXTE*/HEXTE data, from Wilson & Done (2001). We assumed a distance of 2.5 kpc (Sanchez-Fernandez et al. 1999).



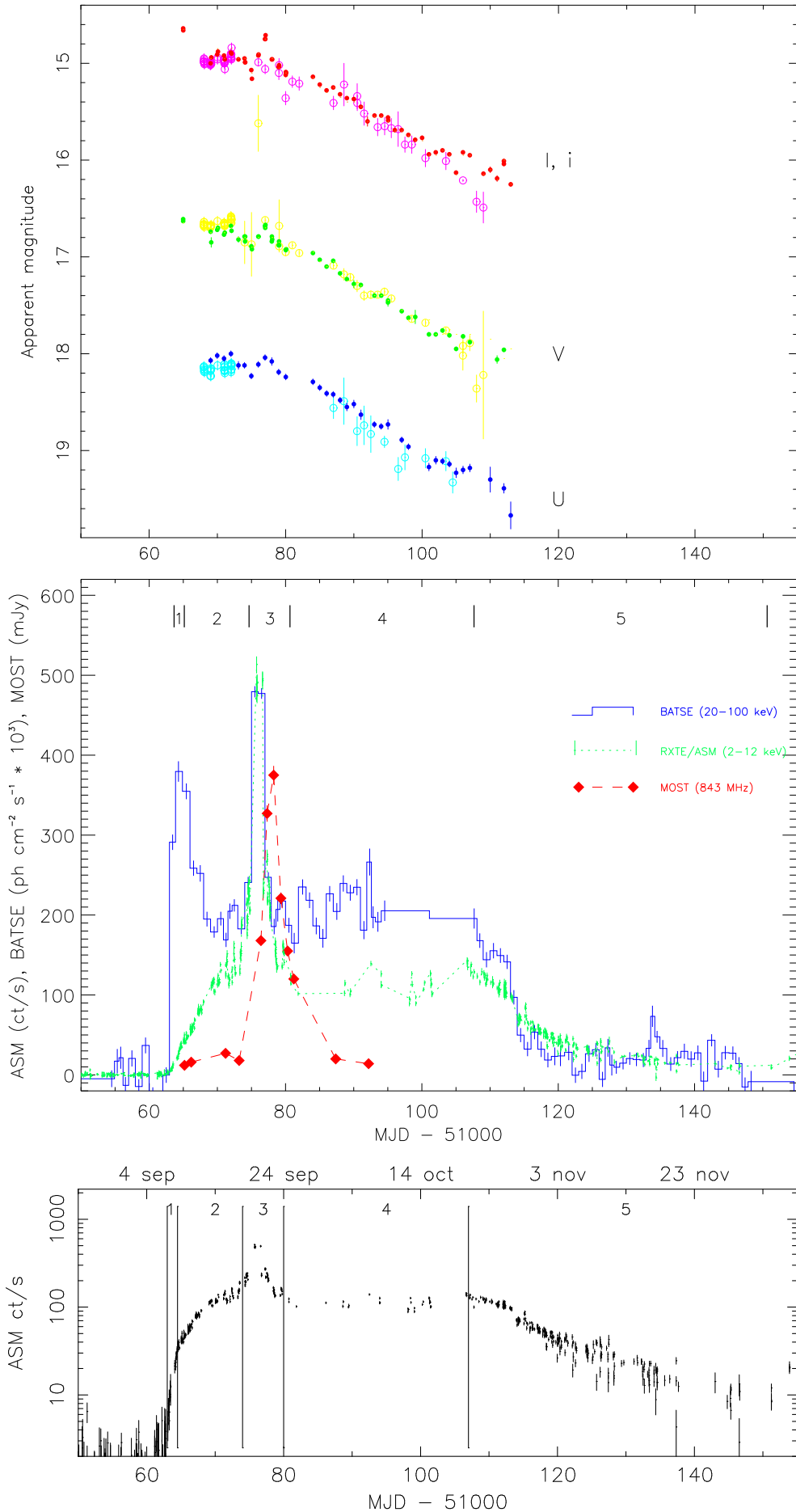


FIG. 1.— Top panel: Optical/IR/UV lightcurves for the 1998 outburst. Open circles: data from Sanchez-Fernandez et al. (1999); filled circles: data from Jain et al. (1999). The upper lightcurve is in the standard *I* band for Jain et al. (1999)’s dataset, and in Gunn *i* for Sanchez-Fernandez et al. (1999)’s. The other two lightcurves are in standard *V* and *U* for both datasets. A possible sharp flare at MJD 51076 was detected in the *V* band by Sanchez-Fernandez et al. (1999), but was not seen by Jain et al. (1999). Central panel: X-ray and radio lightcurves of XTE J1550–564. Bottom panel: the phases of the 1998 outburst sequence shown on a logarithmic plot of the *RXTE*/*ASM* lightcurve.

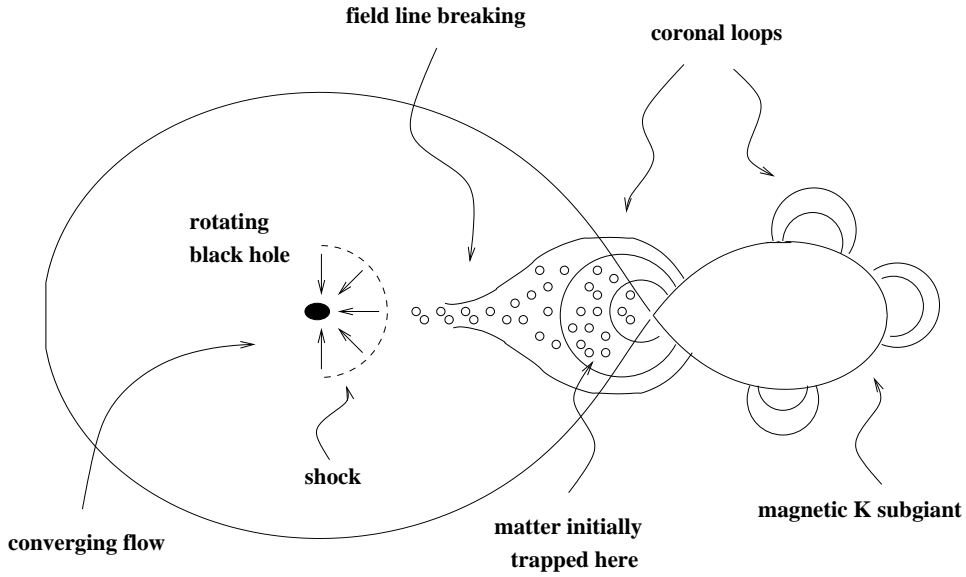


FIG. 2.— A schematic illustration of the magnetic-star model for XTE J1550–564 at the onset of the 1998 outburst. Matter is trapped inside the Roche lobe of the black hole, near the inner Lagrangian point, by the magnetic field of the K subgiant. This provides the initial low angular momentum component of the accretion flow.

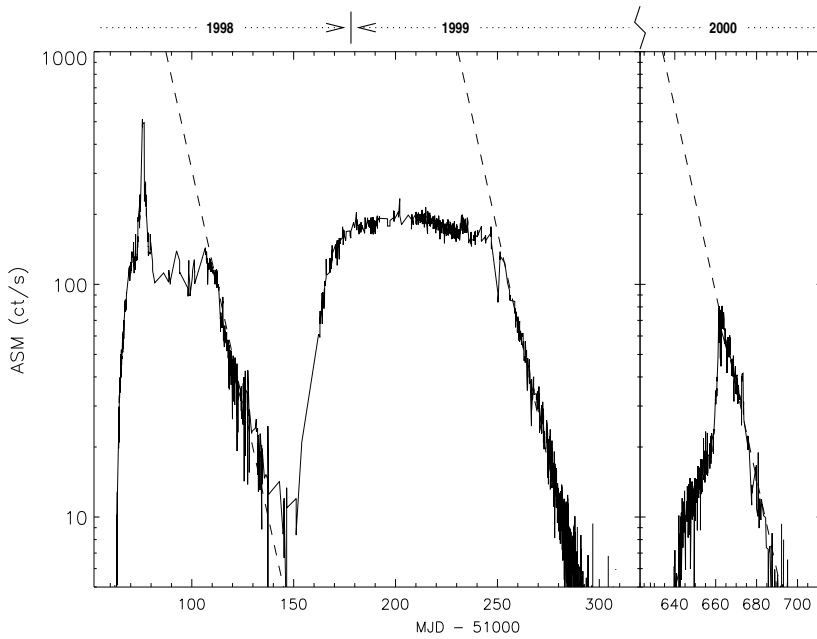


FIG. 3.— The *RXTE*/ASM lightcurves for the three outbursts of XTE J1550–564 between 1998 and 2000. The dashed lines correspond to an exponential decay with an e-folding timescale of 11 days.

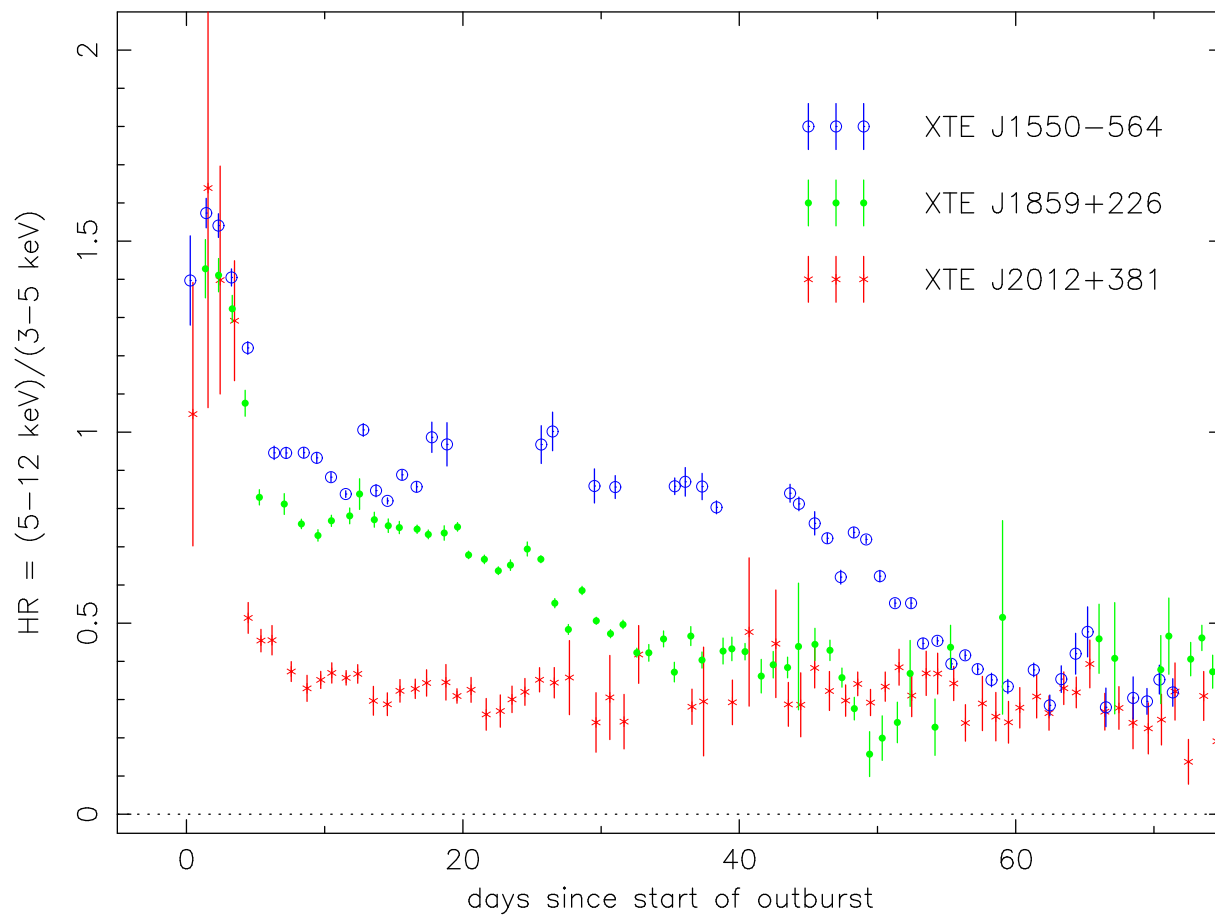


FIG. 4.— Evolution of the *RXTE*/ASM hardness ratios (counts in the 5–12 keV band / counts in the 3–5 keV band) during the outbursts of the BHCs XTE J1550–564 (open circles), XTE J1859+226 (filled circles) and XTE J2012+381 (asterisks). For XTE J1550–564, time = MJD – 50063; for XTE J1859+226, time = MJD – 51459, and for XTE J2012+381, time = MJD – 50956. All three systems show an initial hard spike.